Anisotropic magnetic properties and specific-heat study of a $TbFe_2Si_2$ single crystal

Matúš Mihalik,* Jana Vejpravová, Ján Rusz, Martin Diviš, Pavel Svoboda, and Vladimír Sechovský
Department of Electronic Structures, Charles University, 121 16 Prague 2, The Czech Republic

Marián Mihalik
Institute of Experimental Physics, Slovak Academy of Sciences, Košice 04353, Slovakia
(Received 1 March 2004; published 12 October 2004)

We report on the results of low-temperature magnetization, specific-heat, and resistivity measurements on a $TbFe_2Si_2$ single crystal in magnetic fields up to 5 T applied parallel to the principal crystallographic axes. We conclude that $TbFe_2Si_2$ orders antiferromagnetically below $T_N=5$ K and exhibits strong uniaxial magnetocrystalline anisotropy. Analysis of specific-heat data has revealed a field-dependent Schottky contribution. The observed pronounced magnetocaloric effect points to a strong competition of the applied magnetic field and antiferromagnetic correlations in $TbFe_2Si_2$. Electronic structure of $TbFe_2Si_2$ was studied by first principles calculations in the framework of the density functional theory, which has confirmed the nonmagnetic character of Fe sites.

DOI: 10.1103/PhysRevB.70.134405 PACS number(s): 75.50.−y, 65.40.−b, 75.30.−m

I. INTRODUCTION

$TbFe_2Si_2$ belongs to the isostructural family of the ternary intermetallic compounds RT_2X_2 (R is rare-earth metal, T is transition metal, and X is p metal), which has recently attracted new attention because of the availability of high-quality single crystals. $TbFe_2Si_2$ crystallizes in the body-centered tetragonal crystal structure of the $ThCr_2Si_2$-type with the space group $I4/mmm$. In this structure, the Tb, Fe, and Si atoms occupy the $2a=(0\ 0\ 0)$, $4d=(0\ 1/2\ 1/4)$, and $4e=(0\ 0\ z)$ crystallographic sites, respectively. First powder studies reported the lattice parameters about $a=0.39$ nm and $c=0.99$ nm with the symmetry-free parameter $z_{Si}=0.380$.[1,2] The RT_2X_2 crystal structure consists of basal planes of R, T, and X atoms, respectively, stacked along the c-axis in the sequence $R-X-T-X-R-X-T-X(-R)$, forming a natural multilayer. Such crystal structure often exhibits a strong uniaxial magnetocrystalline anisotropy with magnetic moment confined to the c-axis.

So far, the published data on the thermodynamic properties of $TbFe_2Si_2$ are rather scarce and limited to polycrystalline samples only. First studies[3] of the whole RFe_2Si_2 series reported a weak ferromagnetic order below about 700 K. This result was probably caused by the presence of the ferromagnetic Fe-Si impurity phase, frequently forming at the grain boundaries in the polycrystalline sample. Later on, zero magnetic moment on iron was found by the ^{57}Fe Mössbauer spectroscopy study of the whole RFe_2Si_2 series within the accuracy of the method.[1] The magnetic moment can be then ascribed only to trivalent rare-earth ion, which is subjected to the crystal field of the tetragonal symmetry.

The first powder neutron diffraction experiment[4] on $TbFe_2Si_2$ revealed an incommensurate antiferromagnetic structure of Tb magnetic moments below the Nel temperature $T_N=10.5$ K. Following powder studies[2] allowed researchers to refine the propagation vector of the incommensurate structure as $\mathbf{k}=(0,\ 0.3226,\ 0.1708)$.

A more recent report on investigation of magnetic and transport properties of polycrystalline $TbFe_2Si_2$ claimed different ordering temperature $T_N=6.5$ K and an anomaly on the temperature dependence of magnetic susceptibility at about 180 K suspected for another possible magnetic phase transition.[5]

This rather poor state of the knowledge about $TbFe_2Si_2$ motivated us to grow a good-quality single crystal and subject it to magnetic, specific heat, and electrical resistivity measurements. This paper is reporting results of these experiments. To understand these results well, we investigated the electronic structure of of $TbFe_2Si_2$ by first-principles calculations. We used the general-potential linearized augmented-plane-wave (LAPW) method in order to calculate the ground-state properties (the density of electronic states, the crystal field), which were only partially studied up to now. We went beyond the local-spin-density approximation (LSDA) in the construction of the Kohn-Hohenberg functional[6] and also applied the generalized-gradient approximation, namely, the form of Perdew *et al.*,[7] which is one of the most realistic approaches currently available.

II. EXPERIMENTAL DETAILS AND THEORY

A. Crystal growth

The single crystal of $TbFe_2Si_2$ was grown by the modified Czochralski pulling technique in the tri-arc furnace of the Department of Electronic Structures in Prague. The growth was performed using about seven grams of melt, consisting of the stoichiometric composition of the elemental constituents with the nominal purity: Tb-4N, Fe-3N8, and Si-5N. Because the evaporation rates of terbium, iron, and silicon are similar, no excess of any constituent was necessary to keep the stoichiometric composition of the grown ingot. Using a random necking procedure, low pulling speed (about 8 mm/hr), and a tipped tungsten rod instead of polycrystalline seed (tungsten does not dissolve in the melt), we succeeded to grow a single crystalline ingot about 40 mm long with 5 mm maximum diameter.

The resulting single crystal was very brittle, easily breaking along the basal planes into platelike crystallites. Nevertheless, the x-ray Laue analysis has confirmed high quality of the single-crystalline ingot and no spurious reflections were detected within the Laue pattern. Several rectangular samples with planes parallel to the principal crystallographic planes were then cut from the ingot for studies of magnetic, transport, and thermal properties.

Part of the single-crystalline ingot was pulverized and an x-ray diffraction measurement has been performed on fine powder to determine the lattice parameters and the symmetry-free position of Si atoms. The Rietweld analysis of the powder pattern yielded $a=0.3920$ nm, $c=0.9959$ nm, and $z_{Si}=0.37372$. No traces of foreign impurities were detected within the sensitivity of the method (3%).

B. Magnetization and susceptibility

Magnetization measurements were performed in the temperature range of 2–300 K and in magnetic fields (up to 5 T) parallel to both principal crystallographic axes using the SQUID and PPMS devices (Quantum Design). All data were corrected on the demagnetization factor of the rectangular samples. The detailed inspection of magnetization curves, namely, at higher temperatures, revealed a small, temperature-independent, parasitic ferromagnetic contribution that saturates at about 1 T. Assuming that this contribution comes from the ferromagnetic Fe-Si impurity with the saturated magnetization about 2 μ_B/f.u., we can estimate the amount of this impurity as less than 0.2%, which is well below the resolution of the x-ray diffraction. This results and the fact that the impurity-magnetization is saturated above 1 T and that no phase transition was observed in the impurity phase up to the room temperature enabled us to subtract the impurity contribution from the measured magnetization data.

C. Specific heat

To complete the investigation of basic thermodynamic properties and to determine the magnetic entropy of $TbFe_2Si_2$, the specific heat was studied in detail in zero magnetic field and in magnetic field of 5 T applied along the *c*-axis (the easy axis of magnetization). The measurement was performed in the PPMS apparatus using the temperature-relaxation method, which enables us to accurately determine the heat capacity of small samples with typical mass about 5 mg.

D. Electrical resistivity

Zero-field temperature dependencies of electrical resistivity were measured by the standard four-probe technique for current along the both principal crystallographic axes (*a* and *c*) on rectangular bar-shaped samples in the temperature range of 2–300 K. For the current parallel to the *a*-axis, the cross section was 0.91 mm^2 with the voltage-probes distance 2.13 mm and for the current parallel to the *c*-axis, the cross section was 0.18 mm^2 and the distance of the voltage probes was 0.35 mm, respectively. The easy-cleaving basal planes have frequently caused a spontaneous breaking of the bar sample along the *c*-axis, thus the sample had to be much smaller, and the resistivity along this axis is affected by much larger absolute experimental error (about 4 times). Moreover, frequent microcracks within the basal plane generate a quite large residual resistivity, along the *c*-axis. As both temperature dependencies of resistivity exhibit a minimum at about 10 K, a relative scale related to the respective resistivity at $T=10$ K has been chosen to emphasize the anisotropic behavior of the electrical resistivity in $TbFe_2Si_2$.

E. Electronic structure calculations

For the electronic structure calculations, we used state-of-the-art computational methods, namely, the general-potential linearized augmented plane wave (LAPW, WIEN2k code).[8] The Kohn-Sham equations were solved within the local-spin-density approximation (LSDA), but we also tested the influence of the generalized gradient approximation (GGA).[7] The relativistic effects were treated in the scalar relativistic approximation.[8] Atomic-sphere (AS) radii of 2.8, 2.3, and 1.6 Bohr radii were chosen for Tb, Fe, and Si, respectively. We used about 800 linearized augmented-plane-wave basis functions (about 150 per atom) in the interstitial region and the maximum $l=12$ in the expansion of the radial wave functions inside the AS to represent the valence states. The correlated $4f$ states were treated in the open core approximation, and thus, the terbium $4f$ states are characterized by an integer occupation number $4f$ (Ref. 8). Local orbitals were used to treat the Tb-5*s* and 5*p*, Fe-3*p*, and Si-2*p* states with the valence states in a single energy window. The advantage of this treatment is that the abovementioned semicore states are orthogonal to the valence states. Both the potential and the charge density were expanded inside the spheres into crystal harmonics up to $L=6$ and in the interstitial region into a Fourier series with about 2 500 K stars. For the Brillouin zone (BZ) integration, a modified tetrahedron method[8] with 153 special *k* points in the irreducible wedge (IW) was used to construct the charge density in each self-consistency step. We have carefully checked that with these parameters the calculations converge. The first principles crystal field calculations were performed using the method described in Diviš *et al.*[9]

III. RESULTS AND DISCUSSION

The calculated electronic density of states (DOS) of $TbFe_2Si_2$ using the experimental lattice parameters is shown in Fig. 1(a). The occupied part of the DOS can be decomposed into two regions. The first region, from −10.4 eV to −6.2 eV, consists mainly of Si 3*s* states, which are split off from the main valence band group [see Fig. 1(d)]. There is a band gap from −6.2 eV to −5.3 eV. The bottom of the main valence band group is situated at −5.3 eV. This band group represents mainly the iron 3*d* states with the major part located below the Fermi level (E_F) between −5.3 eV and 2 eV, creating a pronounced broad maximum in the DOS curve from −5.3 eV to E_F, the quasigap situated around E_F, and a secondary maximum around 1 eV [see Fig. 1(c)]. There is some hybridization between

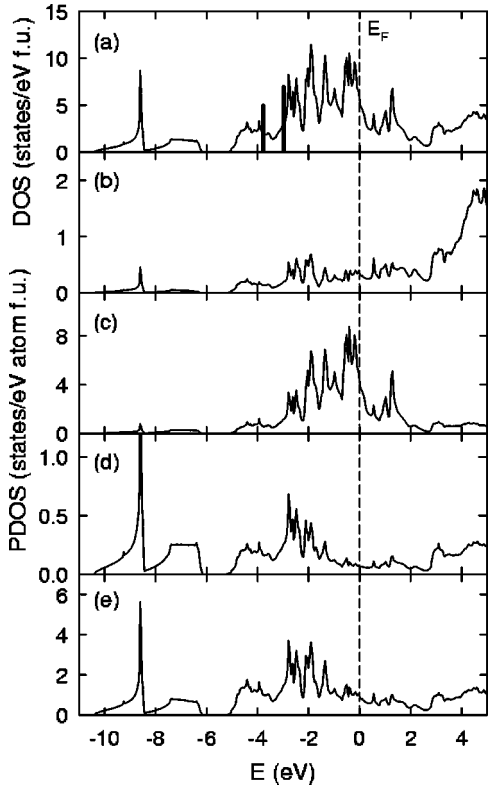

FIG. 1. (a) the calculated DOS, (b, c, d), Tb, Fe, Si-atom projected DOS and (e) the interstitial DOS of the $TbFe_2Si_2$ compound.

Fe-3*d*, Tb-5*d*, and Si-3*p* states present in the energy region between −3 eV and the E_F and a pronounced contribution originating from the interstitial region [see Figs. 1(b)–1(e)]. The energy positions of the localized $4f^6$ ($j=5/2$) and $4f^2$ ($j=7/2$) states—marked by vertical lines—are correctly below the E_F [see Fig. 1(a)].

The E_F is situated at the beginning of the quasigap between the two pronounced maxima in the DOS. The orbital analysis of the DOS shows that mainly Fe-3*d*, Tb-5*d*, and Si-3*p* states are contributing to the total value of DOS at the E_F. The value of the DOS at E_F is smaller than that one that would cause the spontaneous magnetic polarization of the Fe-3*d* states. This peculiar position of the E_F corroborates the idea that the zero Fe magnetic moment observed by Mössbauer spectroscopy[1] is due to the itinerant character of the Fe-3*d* electron states. The value of the DOS at the E_F corresponds to $\gamma=12.5$ mJ/mol K^2, which is lower than the γ value obtained from the analysis of our specific heat data. This points to a rather low value of the mass enhancement coefficient $\lambda=0.76$ related to a small electron-phonon interaction in the $TbFe_2Si_2$ compound.

The low-temperature magnetization curves show large uniaxial magnetocrystalline anisotropy with the *c*-axis as an easy axis of magnetization. The magnetization along the *c*-axis slowly saturates toward the value $\mu_S \sim 9\mu_B$/f.u. (the moment of free Tb^{3+} ion) whreas the *a*-axis magnetization is almost linear, not exceeding $0.5\mu_B$/f.u. in 5 T (see Fig. 2). As the *a*-axis magnetization curves do not show visible temperature dependence between 2 and 10 K, only the 2 K magnetization curve is presented. Assuming the linear dependence of the *a*-axis magnetization, we may estimate the anisotropic field as about 70 T.

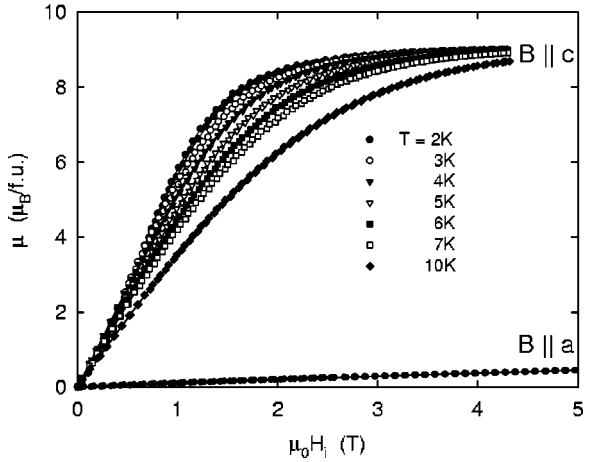

FIG. 2. Magnetization curves of the $TbFe_2Si_2$ single crystal along principal crystallographic axes corrected on the demagnetization factor and on the ferromagnetic impurity. As the magnetization along the *a*-axis does not depend on temperature, only the 2 K curve is shown to simplify the picture.

Closer inspection of the *c*-axis magnetization curves at temperatures below 5 K reveals a metamagnetic transition into a field-induced ferromagnetic state starting at about 0.5 T. To emphasize the effect, Arrott-plots were constructed from the *c*-axis magnetization data. Because to the magnetization curves exhibit a small hysteresis, only data for decreasing field are displayed in Fig. 3. The Arrott-plots for temperatures below 5 K clearly show the typical shape of an antiferromagnet with the metamagnetic transition into the field-induced ferromagnetic alignment of Tb moments.

The temperature dependencies of magnetization along both principal crystallographic directions were measured in the applied fields 2 T and 4 T, respectively. No anomaly was observed around 180 K, which means that reported in Ref. 5 most probably originated in a spurious magnetic phase of poor-quality polycrystalline sample. The data were corrected both for the ferromagnetic impurity and for the demagneti-

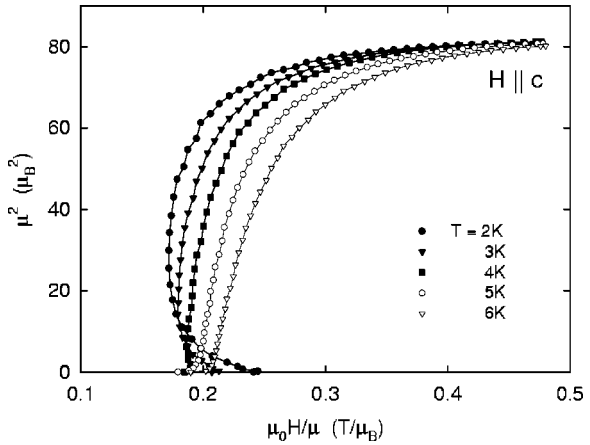

FIG. 3. Arrott plots of magnetization versus field along the *c*-axis for $TbFe_2Si_2$ show a metamagnetic transition at temperatures below 5 K.

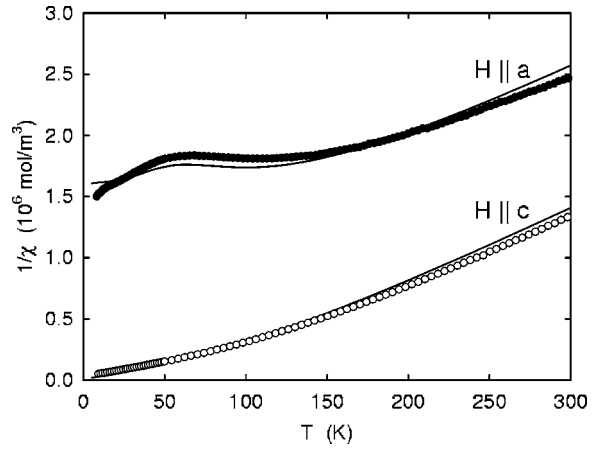

FIG. 4. Temperature dependencies of DC magnetic susceptibility along both principal crystallographic axes corrected on the demagnetization factor and on the ferromagnetic impurity. The lines represents the best theoretical fit.

zation factor and the corresponding dependencies of the magnetic susceptibility were calculated from the data (see Fig. 4). The temperature dependence of magnetic susceptibility along both easy and hard magnetization directions, respectively, document the strong magnetocrystalline anisotropy also in the paramagnetic range. Both susceptibility curves are affected by pronounced crystal-field (CF) effects and cannot be described by the Curie-Weiss law in the measured range. On the other hand, this gives us an opportunity to sensitively fit the CF parameters to the susceptibility data. To analyze CF in $TbFe_2Si_2$, we applied a model Hamiltonian

$$\hat{H}_{CF} = \sum_{l,m} \alpha_l A_l^m \hat{O}_l^m, \tag{1}$$

where $\hat{O}_l^m$ are Stevens CF operators and A_l^m are crystal field parameters and α_l are reduced matrix elements.[10] Diagonalization of such Hamiltonian leads to energy levels of lowest Hund's multiplet splitting in CF. Including Zeeman-like term $H=g_j\mu_B J_z B$ into this Hamiltonian, we can use its eigensystem (energies and eigenstates) to obtain magnetization M as a function of temperature and magnetic field in the following form:

$$M = \frac{\sum_n m_i \exp(-E_n/k_B T)}{\sum_n \exp(-E_n/k_B T)}, \tag{2}$$

where $m_i=\langle u_i|J_z|u_i\rangle$ with E_i and u_i being energies and eigenstates of splitted lowest multiplet, respectively.

The five-dimensional space of CF parameters was scanned to obtain the best fit to the experimental susceptibility data. These data were taken for comparison with the weight $w=1$ at temperatures above 50 K, and with the weight $w=0.5$ at temperatures below 50 K, respectively, due to higher uncertainty in the correction on the magnetic impurity.

Taking into account the different sensitivity of the fitting procedure to the individual CF parameters our best-fit values are: $A_2^0=333\pm5$ K, $A_4^0=-90\pm15$ K, $A_4^4=-350\pm100$ K, $A_6^0=-165\pm25$ K, and $A_6^4=-1750\pm50$ K. This set of CF parameters gives us a good description of the magnetization and susceptibility data. Nevertheless, we can see that the off-diagonal parameters A_4^4 and A_6^4 are rather insensitive to the fitting procedure.

The first principles calculation of the crystal field parameters leads to the following values: $A_2^0=448$ K, $A_4^0=-24$ K, $A_4^4=330$ K, $A_6^0=-1.74$ K, and $A_6^4=18.5$ K using the GGA form of the exchange-correlation potential. The second-order CF parametr A_2^0 has correct sign, which determines the easy c-axis of $TbFe_2Si_2$ in agreement with experiment, and its value is in fair agreement with those derived from analysis of the susceptibility data. The axial parameters A_4^0, A_6^0 have the same signs, but the magnitudes are lower than those derived from analysis of the susceptibility data. The off-diagonal parameters A_4^4 and A_4^6 differ from our best-fit values, but this might originate from the fact that the fitting of magnetic susceptibility is not very sensitive to the values of A_4^4 and A_4^6 parameters. To conclude our first principles calculation of the crystal field interaction provides an important test of our best-fit CF parameters.

Similarly, the effect of the crystal field has to contribute to the specific heat as part of the entropy originates from the crystal-field excitations. In the case of Tb^{3+}, the tetragonal crystal field splits the 13 degenerated levels of the $^7F_6$ ground-state multiplet into 3 doublets and 7 singlets. Contribution to specific heat from the CF splitting can be evaluated by Schottky formula

$$C_{sch} = \frac{R}{T^2}\left[\frac{\sum_{i=0}^{n}\Delta_i^2 \exp(-\Delta_i/T)}{\sum_{i=0}^{n}\exp(-\Delta_i/T)} - \left(\frac{\sum_{i=0}^{n}\Delta_i \exp(-\Delta_i/T)}{\sum_{i=0}^{n}\exp(-\Delta_i/T)}\right)^2\right], \tag{3}$$

where Δ_i is the energy distance of the excited level from the ground-state level in Kelvins.

The specific heat of $TbFe_2Si_2$ (see Fig. 5) is taken as a sum of additive individual contribution: electronic, phonon, and magnetic parts, respectively, where the magnetic part includes both the entropy originating from the CF splitting and the entropy changes due to the magnetic ordering. To perform the accurate analysis of the magnetic part, the detailed information about the electronic and phonon parts is essential.

The simple Sommerfeld term $C_e=\gamma T$ was used for the approximation of the electronic part of the specific heat yielding the value $\gamma=22\pm3$ mJ/mol K^2. On the other hand, full description of the phonon part of the specific heat involves the harmonic approximation of the phonon spectrum using both Einstein and Debye models and the correction for an anharmonicity to accurately approximate the experimental data.[11] Within this approach, the Debye model describes the three acoustic branches of the phonon spectrum and the Einstein model is used for the approximation of the remaining twelve optical branches. To simplify the fit while keeping the model within the experimental error, one triple-degenerated

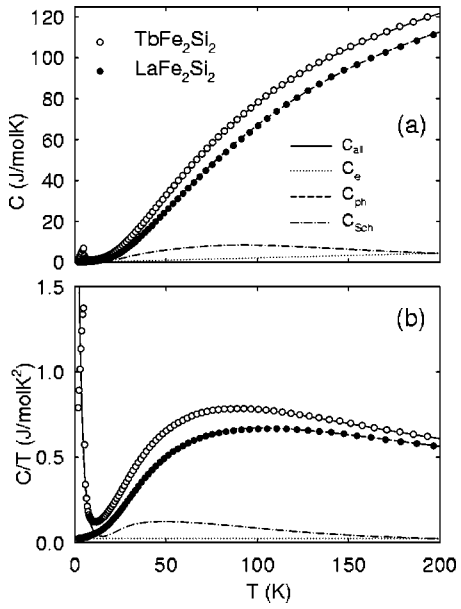

FIG. 5. Temperature dependencies of the specific heat of the $TbFe_2Si_2$ single crystal in a C/T versus T (a) and C/T versus T (b) representation, respectively, in comparison with the nonmagnetic analog $LaFe_2Si_2$. The lines represent the best fit of total, electronic, phonon, and Schottky specific heat, respectively.

acoustic branch and three optical branches with 2-4-6 degeneracy were used instead of the full phonon spectrum, where the 2-4-6 degeneracy follows from the symmetry of the crystal structure. Together with the anharmonicity correction and using $x_N=\Theta_N/T$ for the respective characteristic Θ_N temperature of each branch, this yields the phonon term in the form

$$C_{ph}=R\left\{\sum_{i=1}12\frac{1}{1-\alpha_{Ei}T}\frac{x_{Ei}^2\exp(x_{Ei})}{[\exp(x_{Ei})-1]^2}+\frac{9}{1-\alpha_D T}\left(\frac{1}{x_{Ei}}\right)^3\int_0^{x_{Di}}\frac{x^4\exp(x)}{[\exp(x)-1]^2}\right\},\qquad(4)$$

where α_D and α_{Ei} are the anharmonic correction coefficients for acoustic and optical branches, respectively and R is a gas constant. The best-fit values of the characteristic temperatures and of the anharmonicity coefficients as well as their respective errors are summarized in Table I. The error values of the fit denote the stability of this many-parameter fit within the experimental error of the specific heat data, i.e., the sensitivity of the fit to the individual parameters.

Based on the fit of the nonmagnetic parts, the Schottky analysis of the magnetic part of the specific heat was possible both for the zero-field data and for the 5 T data, respectively (see Fig. 6 and Table II), and the fit well describes the magnetic part of the specific heat in the paramagnetic region. In fact, we see much better agreement of the fit than in the case of magnetic susceptibility. The reason is that the fit of Schottky specific heat depends only on energies of splitting of the ground-state multiplet, which vary in relatively wide interval; thus, it is relatively easily fitted. On the other hand,

TABLE I. Characteristics temperatures and anharmonicity coefficients of multiple degenerated acoustic (D-Debye model) and optical (E-Einstein model) branches of the phonon spectrum yielded by the analysis of the specific heat.

Type of branch	Degeneracy	Characteristic temperature Θ_N (K)	Anharmonicity coefficient α_N (10^{-4} K^{-1})
D	3	183±5	2±1
E_1	6	234±5	5±2
E_2	2	385±10	7±2
E_3	4	515±20	9±3

susceptibility also depends on eigenvectors, and the shape of the calculated susceptibility is much less flexible.

The presence of the magnetic field lifts the degeneracy of the doublets, producing the 13 singlet levels. As can be seen from Fig. 7, with increasing temperature the magnetic entropy in both cases saturates toward $S_m=R\ln 13 \approx 22.3$ J/mol K, which is the entropy of the 13-level system. The low-temperature part of the zero-field magnetic entropy reveals a pronounced plateau at about $R\ln 2$, indicating an isolated quasidoublet as a ground state. Such a well-isolated ground-state quasidoublet (yielded also by the Schottky analysis of the specific heat: $\Delta_1=6.3$ K, $\Delta_2=122$ K) is frequently the origin of strong, Ising-type uniaxial anisotropy in the rare-earth compounds.

Simultaneously, the knowledge of the CF parameters enabled us to directly calculate the CF splitting of the ground-state multiplet. The comparison of the directly calculated and experimental (Schottky analysis) CF splitting is presented in Table II. Considering roughly the 10% error of both calculated and experimental energy-level schemes, we see a good agreement of the calculated and experimental CF splitting.

Finally, the magnetocaloric effect was evaluated directly from the specific-heat data measured in zero and in a magnetic field of 5 T parallel to the c-axis, respectively. The

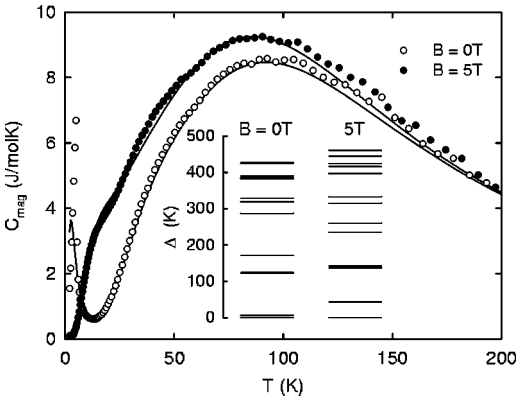

FIG. 6. Low-temperature parts of the magnetic specific heat of the $TbFe_2Si_2$ single crystal in zero field and in magnetic field 5 T along the c-axis. The lines represent the best fits of the Schottky analysis of the data and the inset shows the corresponding crystal-field splitting of the ground-state multiplet in 0 T and in 5 T, respectively.

TABLE II. Results of the Schottky analysis of the specific heat data in the paramagnetic region both in zero magnetic field and in magnetic field 5 T parallel to the *c*-axis yields the crystal-field splitting of the $^7F_6$ ground-state multiplet of $TbFe_2Si_2$. The zero-field CF splitting is compared to the calculated one Δ_i calc., where the calculation is based on the model Hamiltonian (1).

i	Δ_i (B=0 T) (K)	Δ_i (B=5 T) (K)	Δ_i calc (B=0 T) (K)
0	0	0	0
1	6.3±1	43±4	5±1
2	122±13	137±15	117±36
3	122±13	142±15	117±36
4	171±20	235±25	279±37
5	287±30	260±25	295±29
6	319±30	315±30	295±29
7	329±35	333±30	311±25
8	383±40	397±40	324±29
9	383±40	416±40	343±33
10	390±40	424±40	459±27
11	425±45	445±45	459±27
12	425±45	461±45	497±25

magnetocaloric effect represents either an isothermal change of entropy ΔS or an adiabatic change of temperature ΔT, respectively, corresponding to a change of magnetic field ΔB (see Fig. 8). The isothermal change of entropy is negative in the low temperature region, which is consistent with the field-induced ferromagnetic alignment of the Tb moments, significantly lowering the entropy of the system. The temperature dependence of the adiabatic change of temperature exhibits a pronounced maximum at about 6 K, where the temperature change is almost 4 K/T.

The temperature dependencies of resistivity measured along both principal axes (see Fig. 9) show local minima at about 10 K. Below 10 K the resistivity increases with decreasing temperature, which can be ascribed to the onset of the antiferromagnetic short-range ordering. This increase terminates around 4 K, which is below T_N. Different temperature dependencies of resistivity can be observed in the ordered region. While the *a*-axis resistivity is almost temperature independent below 4 K, the resistivity along the *c*-axis exhibits a maximum at about 3.5 K. In the paramagnetic region above 10 K, the resistivity along both axes can be described using the Bloch-Grüneissen formula

$$\rho_{phon} = \rho_0 + C\left(\frac{T^5}{\Theta_D^4}\right)\int_0^{\Theta_D/T} \frac{x^5 dx}{(\exp x - 1)[1 - \exp(-x)]}, \tag{5}$$

where ρ_0 is a residual resistivity, C is a temperature independent factor proportional to the electron-phonon interaction, and T_D is the mean Debye temperature. The fit yields T_D about 330±20 K for both resistivity dependencies. Note that T_D in this formula represents the characteristic temperature of the whole phonon spectrum and is different from the characteristic temperature of the acoustic phonons Θ_D from the phonon-specific-heat analysis.

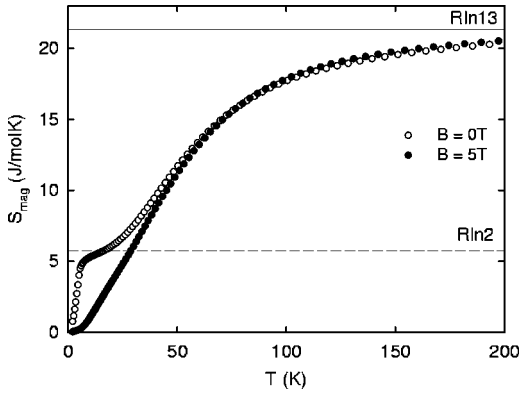

FIG. 7. Temperature dependencies of magnetic entropy of the $TbFe_2Si_2$ single crystal in 0 T and in magnetic field 5 T along the *c*-axis. The horizontal lines represent the entropy of the doublet and of the 13-level system.

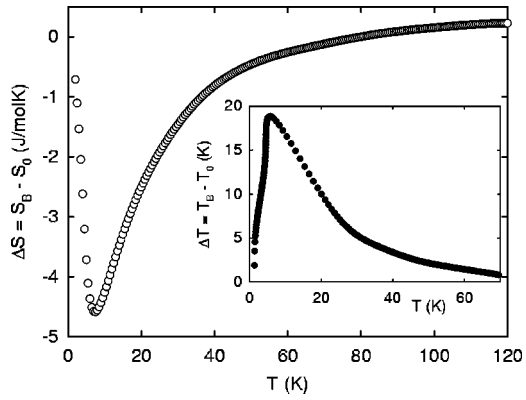

FIG. 8. Temperature dependence of the isothermal change of entropy corresponding to the change of magnetic field from 0 to 5 T. Temperature dependence of the corresponding adiabatic change of temperature is presented in the inset.

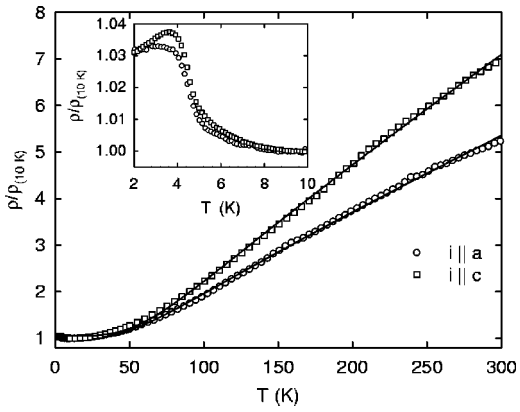

FIG. 9. Temperature dependencies of relative electrical resistivity of the $TbFe_2Si_2$ single crystal with current along both principal crystallographic axes. The inset shows the low-temperature detail. The resistivity data are related to the respective resistivity at 10 K (see text) to better visualize the anisotropy of the resistivity.

IV. CONCLUSION

In conclusion, we have succeeded to grow a good-quality single crystal of $TbFe_2Si_2$ and measured its magnetization, specific heat, and electrical resistivity behavior. This compound exhibits a strong uniaxial magnetocrystalline anisotropy with crystallographic *c*-axis as the easy axis of magnetization. $TbFe_2Si_2$ orders antiferromagnetically below the $T_N = 5$ K. The low ordering temperature points to rather weak antiferromagnetic interaction, which was confirmed by the observation of the metamagnetic transition into the field-induced ferromagnetic alignment of Tb magnetic moments in magnetic fields above 0.5 T parallel to the easy axis. Simultaneously, the strong magnetocrystalline anisotropy helps to keep the parallel alignment of the magnetic moments, yielding a significant change of entropy between the antiferromagnetic and the field-induced ferromagnetic state. The first principles calculation based on DFT provides the information about the electronic structure and crystal field interaction of $TbFe_2Si_2$ compound.

A pronounced crystal-field effect was observed in the paramagnetic region both on the specific heat and on the magnetic susceptibility. The Schottky analysis of the specific heat yields the total crystal-field splitting of the ground-state multiplet of about 400 K with the isolated quasidoublet of about 6 K as a ground state. The temperature dependence of the magnetic susceptibility does not show a Curie-Weiss behavior in the measured temperature range and the anisotropy of the susceptibility in the paramagnetic range can be described using the crystal-field model.

ACKNOWLEDGMENTS

This work is part of the research program MSM113200002 that is financed by the Ministry of Education of the Czech Republic. Part of this work was also supported by the Grant Agency of the Czech Republic (Grant No. 106/02/0940) and VEGA of the Slovak Republic No. 2/4050/04.

*Electronic address: mmihalik@saske.sk

[1] D. R. Noakes, A. M. Umarji, and G. K. Shenoy, J. Magn. Magn. Mater. **39**, 309 (1983).
[2] W. Bazela, J. Leciejewicz, H. Ptasiewiczbak, and A. Szytula, J. Magn. Magn. Mater. **72**, 85 (1988).
[3] A. Szytula and J. Leciejewicz, in *Handbook on the Physics and Chemistry of Rare Earths*, edited by K. A. Gschneidner and L. Eyring (North-Holland, Amsterdam, 1989), Vol. 12, Chap. 83.
[4] H. Pinto, M. Melamud, M. Kuznietz, and H. Shaked, Phys. Rev. B **31**, 508 (1985).
[5] H. M. Duh, I. S. Lyubutinz, Y. C. Cheny, H. F. Cheny, and C. H. Liny, J. Phys.: Condens. Matter **10**, 4457 (1998).
[6] J. P. Perdew and Y. Wang, Phys. Rev. B **45**, 13 244 (1992).
[7] J. P. Perdew, K. Burke, and M. Ernzerhof, Phys. Rev. Lett. **77**, 3865 (1996).
[8] P. Blaha, K. Schwarz, G. Madsen, D. Kvasnicka, and J. Luitz, *WIEN2k* (Vienna University of Technology, Vienna, 2001).
[9] M. Diviš, J. Rusz, G. Hilscher, H. Michor, P. Blaha, and K. Schwarz, Czech. J. Phys. **52**, 283 (2002).
[10] M. T. Hutchings, Solid State Phys. **16**, 227 (1964).
[11] P. Svoboda, P. Javorský, M. Diviš, V. Sechovský, F. Honda, G. Oomi, and A. A. Menovsky, Phys. Rev. B **63**, 212408 (2001).